ACS NANO

www.acsnano.org

ARTICLE

Layer Number Dependence of Li^+ Intercalation on Few-Layer Graphene and Electrochemical Imaging of Its Solid–Electrolyte Interphase Evolution

Jingshu Hui,[†,‡] Mark Burgess,[‡] Jiarui Zhang,[‡] and Joaquín Rodríguez-López*[,‡]

[†]Department of Materials Science and Engineering, University of Illinois at Urbana-Champaign, 1304 West Green Street, Urbana, Illinois 61801, United States

[‡]Department of Chemistry, University of Illinois at Urbana-Champaign, 600 South Mathews Avenue, Urbana, Illinois 61801, United States

Supporting Information

ABSTRACT: **A fundamental question facing electrodes made out of few layers of graphene (FLG) is if they display chemical properties that are different to their bulk graphite counterpart. Here, we show evidence that suggests that lithium ion intercalation on FLG, as measured *via* stationary voltammetry, shows a strong dependence on the number of layers of graphene that compose the electrode. Despite its extreme thinness and turbostratic structure, Li ion intercalation into FLG still proceeds through a staging process, albeit with different signatures than bulk graphite or multilayer graphene. Single-layer graphene does not show any evidence of ion intercalation, while FLG with four graphene layers displays limited staging peaks, which broaden and increase in number as the layer number increases to six. Despite these mechanistic differences on ion intercalation, the formation of a solid–electrolyte interphase (SEI) was observed on all electrodes. Scanning electrochemical microscopy (SECM) in the feedback mode was used to demonstrate changes in the surface conductivity of FLG during SEI evolution. Observation of ion intercalation on large area FLG was conditioned to the fabrication of "ionic channels" on the electrode. SECM measurements using a recently developed Li-ion sensitive imaging technique evidenced the role of these channels in enabling Li-ion intercalation through localized flux measurements. This work highlights the impact of nanostructure and microstructure on macroscopic electrochemical behavior and provides guidance to the mechanistic control of ion intercalation using graphene, an atomically thin interface where surface and bulk reactivity converge.**

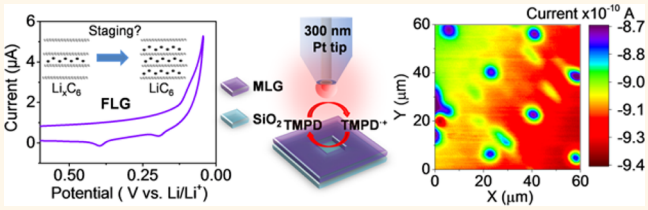

KEYWORDS: *graphene, layer number dependence, Li intercalation, SEI, staging mechanism, SECM*

Li-ion batteries are a mature rechargeable energy storage platform that utilizes the reversible intercalation of Li^+ into carbonaceous materials and transition metal oxides used as anodes and cathodes, respectively. Graphite's intrinsic layered structure has made this material a workhorse in the battery community for Li-ion battery anodes. In the past few decades, research on the layered properties of graphitic anode materials has focused on exploring its intercalation mechanisms,[1−3] solid–electrolyte interphase (SEI) formation, composition and structure,[4−6] and ways to improve its structural stability and cyclability.[7−9]

The emergence of carbon-based two-dimensional materials, such as electrodes composed of few layers of graphene (FLG),[10−12] have prompted the search for materials with a distinct or superior performance toward intercalation than that of bulk graphite. Arguments for improvements over graphite tend to gravitate toward the enhanced electrical properties of graphene, their large surface area, or their processability.[13−16] However, other fundamental differences in the intercalation mechanism of Li^+ on FLG can be proposed. Here, we address the question of whether graphite's bulk properties for Li^+ intercalation and SEI formation are maintained in a carbon material with a finite number of layers, or if they take on electrochemical properties unique to themselves.

The Li^+ intercalation process into graphite follows a staging mechanism, in which Li ions do not randomly insert into any available empty interlayer galleries simultaneously, but instead intercalate into specific interlayers at a time.[17−20] It has been

Received: December 7, 2015
Accepted: March 4, 2016
Published: March 4, 2016

ACS Publications © 2016 American Chemical Society

DOI: 10.1021/acsnano.5b07692
ACS Nano 2016, 10, 4248–4257

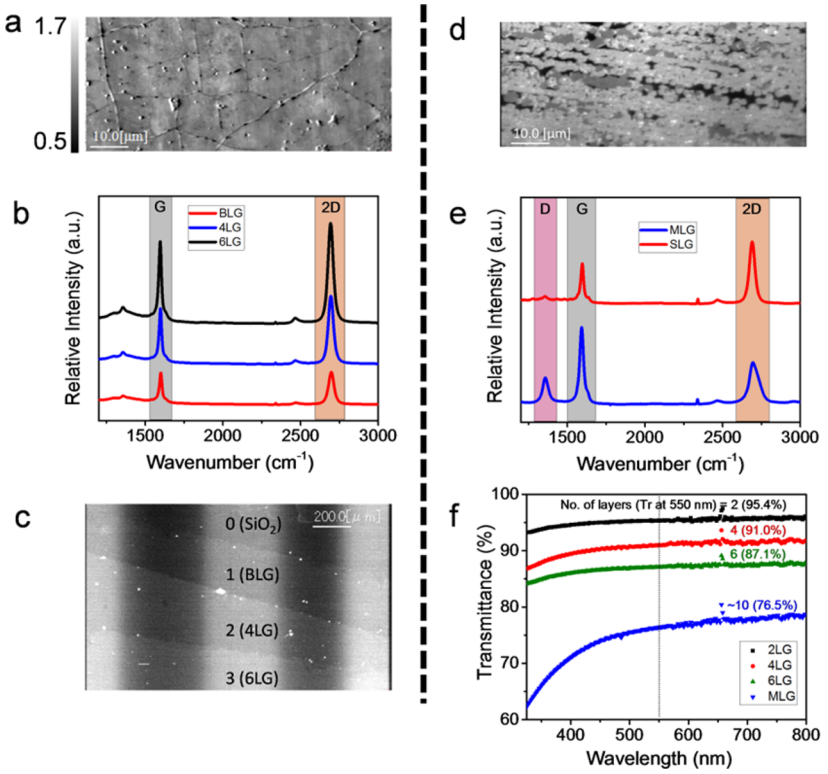

Figure 1. Spectroscopic characterization of FLG samples. (a) Raman 2D/G intensity ratio mapping of CVD-grown BLG sample on Si/SiO_2 wafer. The graphene is primarily composed of double layers with tens of micrometer grain size. (b) Raman spectra of layer-by-layer transferred samples: BLG, 4LG, and 6LG. Each transfer maintained the 2D/G intensity ratio double layer characteristics of BLG but contribute to accumulated spectrum intensity. (c) Raman 2D intensity mapping of multiple graphene transfers. From top to bottom: SiO_2, 1 time transferred BLG, 2 times transferred 4LG, 3 times transferred 6LG, respectively. Each layer can be easily identified through its intensity change and the observed sharp edges between layers. (d) Raman 2D intensity mapping of directly grown MLG sample. The sample consisted mostly of micrometer sized MLG domains (bright region), decorated with few SLG (gray region) and holes (black region). The Raman spectra of MLG and SLG region is shown in (e). (f) UV−vis transmittance of layer-by-layer transferred BLG, 4LG, and 6LG samples, together with directly grown MLG samples (~10 layers).

reported that Li ions first randomly occupy available sites (dilute stage-1, LiC_{72}), then diffuse to fill every four layers of the graphene planes (stage-4, LiC_{36}), and finally concentrate to fill every three (stage-3, LiC_{27}), two (stage-2, LiC_{12}), and one (stage-1, LiC_6) layer(s), respectively.[8,21] Thus, in graphite the intercalation process is strongly dependent on the number of neighboring delithiated interlayers at any given time. FLG naturally displays limited numbers of available intercalation sites; therefore, we hypothesize that the staging of lithiation will be necessarily limited as certain charge stages are not accessible. For example, stage-4 may not be possible in FLG with less than 5 layer graphene. With limited interlayers for Li^+ intercalation in FLG, this process might reveal different phase transitions between stages and a deviation from intercalation potentials when compared to bulk graphite.

Apart from Li^+ intercalation, a SEI is also generated at the early stages of cycling on graphite anodes. The SEI forms because the negatively polarized anode causes the degradation of electrolyte and solvent, causing deposition of inorganic and organic decomposition products, onto the surface of the graphite. However, after formation and stabilization, the SEI layer prevents further degradation of electrolyte and solvent as this layer is largely electronically insulating, thus blocking electron transport across it.[4−6] Yet even with the SEI completely formed, the anode maintains high Li^+ conductivity which ensures long-term cyclability. Compared to graphite, FLG has similar surface properties and electrochemical characteristics;[22] thus, it may exhibit similar SEI formation processes. However, the stability of the SEI on FLG, together with its electronic and ionic conductivity properties, has not been fully addressed.

In this paper, we explored Li^+ intercalation and SEI formation on FLG *via* stationary voltammetry and electrochemical imaging methods. Two synthetic routes were used to fabricate FLG. One consisted of the direct growth of multilayer graphene (MLG), which had on average 10 graphene layers. The other methodology consisted of the layer-by-layer transfer of bilayer graphene (BLG), to controllably produce layered number graphene samples (2−6 layers). FLG samples revealed a layer number dependence for the number and location of intercalation peaks, which is representative of the existence of a staging-type mechanism.

Previous studies of the SEI on graphite were focused on the structural, compositional and stability changes with different carbon materials, solvents, electrolytes, and temperatures using spectroscopic and microscopic methods such as X-ray photoelectron spectroscopy,[23,24] Fourier transform infrared spectroscopy,[25] mass spectrometry,[24] X-ray diffraction,[26] and electron microscopy.[24] Electrochemical impedance spectroscopy (EIS) is the most common method to explore SEI's conductivity after formation, but the information from these experiments is spatially averaged.[27] Here, we introduce scanning electrochemical microscopy (SECM) to visualize *in situ* the local electronic transfer and ionic transport properties of FLG

DOI: 10.1021/acsnano.5b07692
ACS Nano 2016, 10, 4248−4257

electrodes after SEI formation. SECM is a powerful tool to image highly localized substrate electrochemical processes, and provides a convenient platform to test comparisons between materials and substrate conditions within the same experiment. In our experiment, a Pt nanoelectrode was used to sense and image local electrochemical kinetic changes before and after SEI formation through SECM feedback experiments. Additionally, a Hg-capped Pt ultra-micro electrode was used as a spatially resolved selective Li-ion sensor *via* stripping voltammetry[28] to explore Li^+ uptake into FLG with a formed SEI layer. Spatially resolved information about electron transfer kinetics and ionic transport of SEI coated MLG samples provided details of SEI layer behavior changes *in situ*, and guided us to better understand the SEI properties on ultrathin FLG samples.

RESULTS AND DISCUSSION

To explore Li^+ intercalation into FLG with different number of layers, two different types of graphene substrates were grown using chemical vapor deposition (CVD). One CVD method reliably produced double layer graphene, which, after layer-by-layer transfer, yielded graphene with 2, 4, or 6 layers as needed. The other CVD method directly grew multilayer graphene. Figure 1 summarizes the properties of different graphene samples. The Raman 2D/G ratio mapping in Figure 1a reflects the double layer structure of graphene, which displays a 2D/G intensity ratio around 1.[29,30] Graphene samples showed a uniform and continuous sheet with tens of micrometer domain size. After layer-by-layer transfer of bilayer graphene sheets, 2-, 4-, and 6-layer graphene substrates were obtained. Figure 1c is the Raman 2D intensity mapping of a three times transferred graphene sample where each layer can be recognized with sharp edges, indicating the integrity of these samples was maintained after a layer-by-layer wet transfer. A zoomed-in view of each layer, the Raman spectra of 1, 2, and 3 times transfer graphene samples are shown in Figure 1b. From these spectra, it is clear that each layer preserved a 2D/G intensity ratio of about 1, and double and triple transferred samples exhibited 2 or 3 times higher intensities.[31] With this method, we can successfully manufacture bilayer graphene (BLG), 4-layer graphene (4LG), and 6-layer graphene (6LG) samples verified by Raman analysis. Figure 1d shows the Raman 2D intensity mapping of directly grown multilayer graphene (MLG), where Raman spectra of representative areas in MLG are shown in Figure 1e. In this figure, the white areas are multilayer graphene domains, gray areas are single-layer domains, and black areas are holes. Additional methods were used to characterize graphene samples for verification. The gradual decrease of UV−vis transmittance (Figure 1f) for the progression from single, double, and triple layer-by-layer transferred bilayer graphene on glass agrees well with Raman images. According to previous reports, each layer of graphene contributes to a 2.3% transmittance decrease at 550 nm,[32] as quantitatively observed for our 2-, 4-, and 6-layer graphene sheets. From the transmittance data of MLG (~76%), this material was roughly equivalent to 10 layers of graphene.

After successfully making the graphene samples (2-, 4-, 6-layer graphene and directly grown multilayer graphene), photolithography and reactive ion etching methods were applied to create ionic openings for Li^+ to intercalate in-between graphene sheets. The fabrication procedure is summarized in Figure 2a: the graphene on Si/SiO_2 wafer sample ① went through one step photolithography to create 3 μm round windows on S1813 photoresist ②, RIE etching of

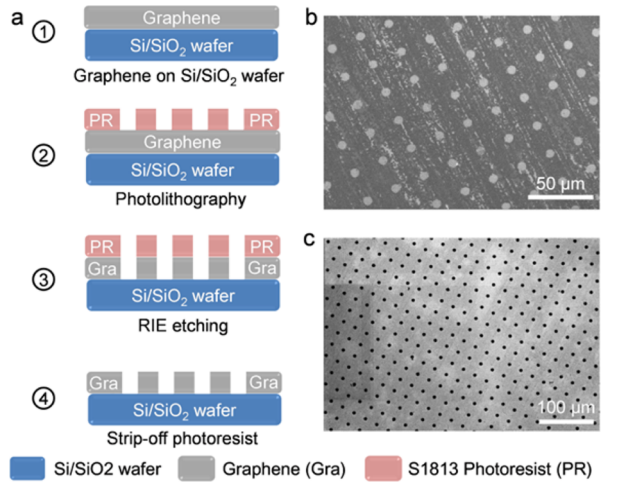

Figure 2. FLG patterning procedure and results. (a) Schematic procedure to create point of entry holes for ionic intercalation on FLG. Graphene samples ① were patterned *via* photolithography with S1813 as photoresist, leaving patterned 3 μm window openings ②. Oxygen plasma was applied to etch exposed graphene area ③. After carefully removing photoresist, patterned openings were generated on FLG sample ④. (b) SEM image of patterned MLG sample. (c) SEM image of patterned SLG sample (exfoliated BLG sample). This last image was taken after days of electrochemical experimentation with SLG.

exposed graphene under S1813 windows ③, and stripping off the rest of photoresist to yield patterned graphene samples ④. As shown in Figure 2b,c, the patterned openings were imbedded into the graphene basal planes and generated additional edge planes for Li^+ to intercalate. Figure 2b is the SEM of patterned MLG before intercalation test which matches well with the Raman image in Figure 1d. Figure 2c is the SEM image of patterned "bilayer graphene" after days of experimentation in electrolyte. The graphene sheets maintained their integrity without any obvious mechanical damage. However, as discussed later in more detail, after the entire patterning process, the top layer of bilayer graphene peeled off and left only the bottom layer on Si/SiO_2 wafer intact, which is referred as a patterned SLG later. The stripping of the top graphene layer might originate from the strain generated from the Si/SiO_2 substrate,[33] which decreases the attraction between bottom and top basal planes. The stripped top graphene layer came off during the acetone rinsing step that removes the photoresist, thus BLG was not obtained for electrochemical experiments. Instead we used the resulting SLG surface.

We first examined Li^+ intercalation into MLG. The first several full CV cycles of MLG are shown in Figure 3a, and can be divided into two regions: SEI formation and Li intercalation, in which the zoomed-in results are shown in Figure 3b,c. The SEI formation region is mainly located between 3.0 and 0.4 V *vs* Li/Li^+ and has multiple peaks and evolution with cycling that match well with previously reported results of graphite.[4,34] Only a small portion of SEI processes which rapidly fade upon cycling contribute to the background in the Li^+ intercalation regime.[6] In the first cycle (red curve in Figure 3b), the SEI formation was activated on the MLG surface. Due to the self-passivating nature of the SEI, less of it was generated with each subsequent cycle until no new growth is evident after the sixth cycle (highlighted as green curve in Figure 3b). In comparison, the Li^+ intercalation region in Figure 3c had much less change from cycle-to-cycle, nearly maintaining the same current levels

DOI: 10.1021/acsnano.5b07692
ACS Nano 2016, 10, 4248−4257

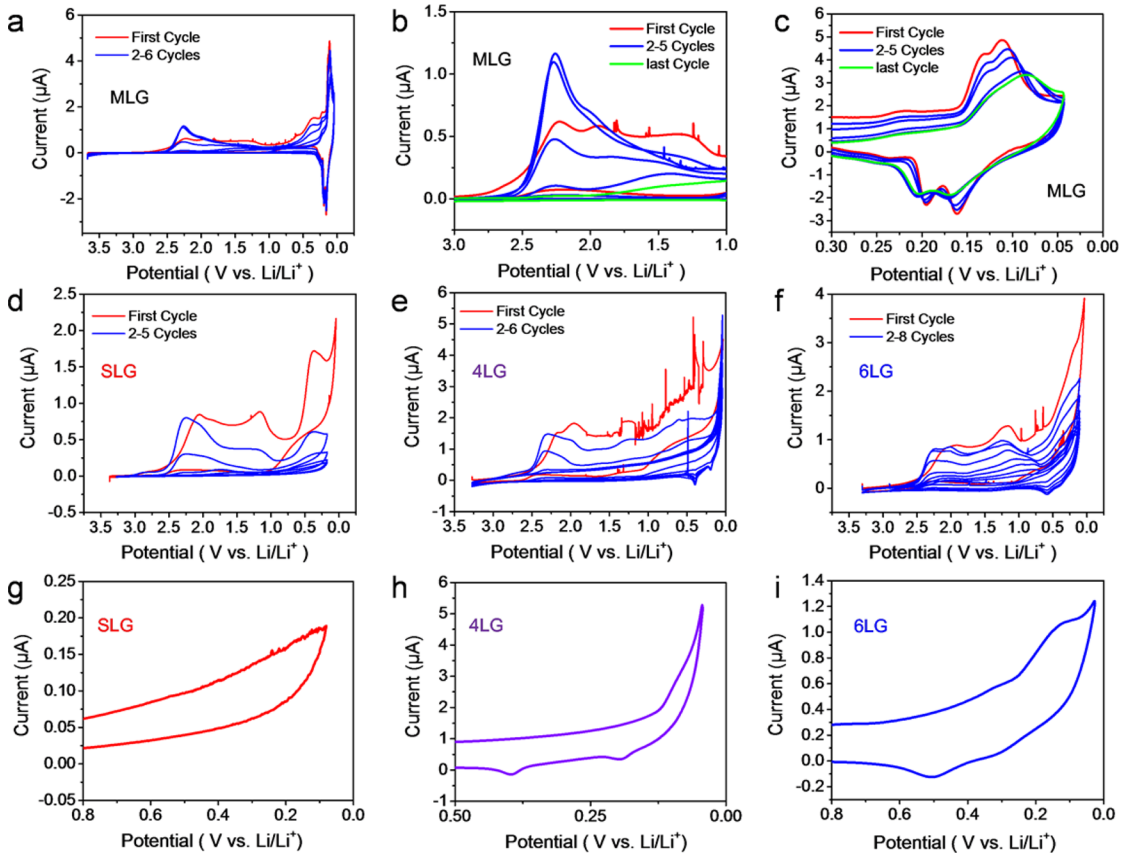

Figure 3. Cyclic voltammograms of FLG. (a) Cycling behavior of MLG; the first cycle is labeled with red color to distinguish it from following cycles in blue. The zoomed in figures of SEI region and Li^+ intercalation region are shown in panels b and c, respectively. In panels b and c, the sixth (last) cycle is labeled in green. (d) Cycling behavior of patterned SLG sample with first cycle labeled in red. After stabilization, the last cycle in the intercalation region is shown in panel g. Similarly, panels e and h, and f and i are the full cycling CVs and stabilized intercalation behaviors for 4LG and 6LG, respectively. Test condition: 0.1 M $LiBF_4$ in 50:50 ratio PC/EC; electrode area was 4.9 mm^2.

and intercalation potentials. Comparing the first cycle (red curve in Figure 3c) to previous studies on graphite with a submicrometer thickness,[21] we can assign the three intercalation peaks at 0.22, 0.14, and 0.11 V to changes between dilute stage 1 to stage 4, stage 3 to stage 2, and stage 2 to stage 1, respectively. For all of the scan rates in CV tests of FLG samples, we chose a scan rate of 1 mV/s. Previous studies on ultrathin graphite materials have been performed up to hundreds of times slower; however, the fast diffusion of Li in FLG makes the relatively high scan rate possible while still maintaining distinguishable CV signals.[35] On FLG with more than 10 layers, *i.e.*, MLG, the full spectrum of Li insertion staging steps is observed, consistent with bulk graphite. This result substantiates our hypothesis that fewer layer graphene electrodes are required to explore the early state staging mechanisms.

Preliminary studies of Li^+ intercalation on unpatterned BLG, 4LG and HOPG (highly oriented pyrolytic graphite) showed no clear evidence of this process due to the low mechanical defect density of the samples used. Figure S1 shows voltammograms of these samples where unstable electrochemical signals were obtained, and often exfoliation was observed. It is known that the intercalation of Li ion occurs through the edge plane of graphite, such that high-quality pristine unpatterned FLG electrodes do not contain enough points of access for Li ion insertion.[36] When patterned, SLG, 4LG, and 6LG displayed contrasting intercalation signatures. Full CVs of the first several cycles of these three samples are shown in Figure 3d–f. They all display a similar SEI evolution region between 3.0 and 0.4 V, but have diverse intercalation properties between 0.4 and 0 V. In all three curves, the SEI formation follows the same trend as MLG where there is an initial conditioning and growth which eventually stabilizes after several cycles. Similar conditioning steps also appeared in the Li^+ intercalation regions of patterned SLG, 4LG, and 6LG. The steady intercalation behaviors for these samples are summarized in Figure 3g–i, which displays the last voltammetric cycle in each. As expected, due to the lack of galleries found between adjacent graphene sheets, in SLG (Figure 3g) no intercalation occurs. While we cannot discard a contribution from adsorbing ions or Li plating to the electrode, intercalation peaks were not observed. The peak observed for SLG around 0.4 V in the first cycle can still be attributed to SEI formation, since the position matches well with the SEI peak observed at 0.4 V in MLG. Additionally, this signal fades and is not observable in subsequent cycles (Figure 3d).

In contrast to SLG, patterned 4LG and 6LG (Figure 3h,i) have clearly observable intercalation/deintercalation peaks. The intercalation and deintercalation peak ranges are summarized in Table S1 and Figure S3. Since there are only four graphene sheets in 4LG, two deintercalation peaks reflect the changes between stages 3/2, and 2/1, observed at 0.4 and 0.2 V, respectively. However, in the intercalation region only one broad peak exists. We note a similar phenomenon for MLG,

DOI: 10.1021/acsnano.5b07692
ACS Nano 2016, 10, 4248–4257

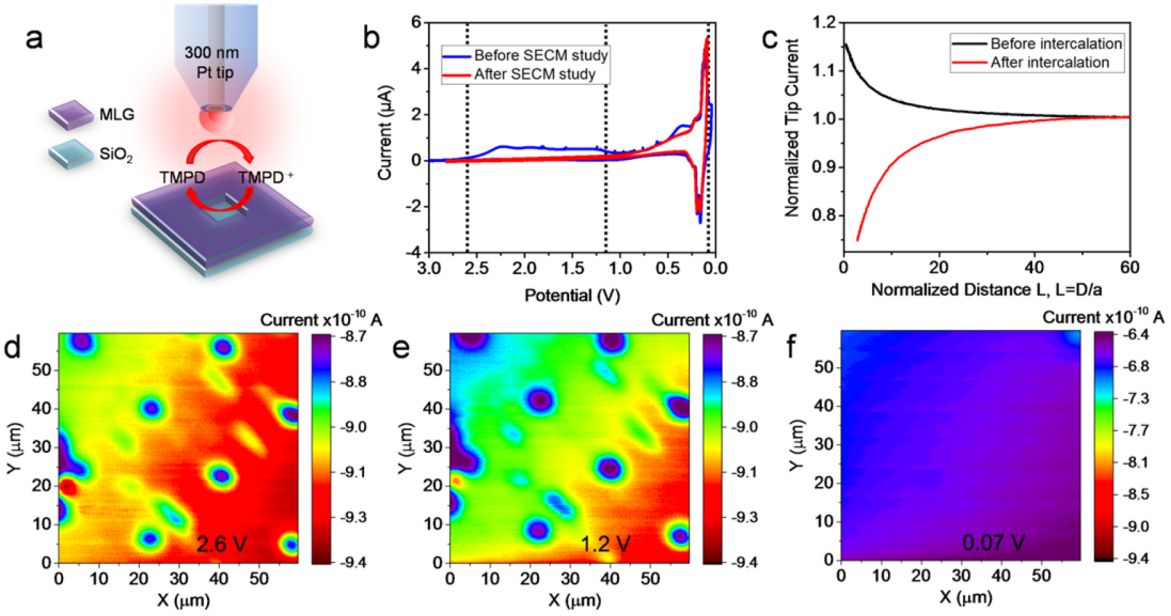

Figure 4. Feedback SECM imaging of SEI formation on fresh patterned MLG. (a) Schematic diagram of SECM feedback mode for the imaging of patterned MLG. The SECM tip was scanned over the substrate at 133 nm of tip−substrate distance. *N,N,N′,N′*-tetramethyl *p*-phenylenediamine (TMPD) was used as a redox mediator. This species was oxidized at Pt tip, while MLG reduced it back, generating a feedback signal. (b) CVs comparing a fresh patterned MLG substrate (blue) and after SECM experimentation (red) showed no change in the intercalation signatures, but a fully developed SEI with no further electrochemical evidence of growth at the end of the experiment. The dashed lines represent the selected substrate potentials for imaging, chosen to be before and during SEI formation. (c) Tip approaching curves to MLG surface before/after SEI formation, which indicate that the fresh MLG surface is electroactive while the formation of the SEI layer blocks electron transfer. The limiting tip current far from the substrate was 9.3×10^{-10} A. (d−f) SECM feedback images of TMPD at various substrate potentials listed in each panel; the current changes reflect the changes in substrate kinetics following SEI formation.

shown in Figure 3c, in which the two intercalation peaks at 0.14 and 0.11 V (red curve) gradually merge into one broad peak (green curve). Consequently, the two intercalation peaks in 4LG could presumably also combine into one signal. However, the reason for this merging of peaks might be of different origin. In MLG at least, the evolution of intercalation peaks suggests that it might come from a conditioning of the material, where structural changes induced by multiple Li ion insertions and extractions lead to a distribution of intercalation sites. When the direction of the potential sweep is reversed, the back diffusion and deintercalation of Li ion is largely controlled by the intrinsic properties of the already lithiated graphene electrode, thus yielding discrete deintercalation peaks. As the layer number of graphene is increased to 6 layers, there are sufficient graphene sheets for all four staging states to be observed.

From Table S1 and Figure 3c,h,i, we noticed a continuous shift of first and second deintercalation peaks among 4LG, 6LG, and MLG. Assuming MLG represents mostly bulk graphite's properties, the positive potential shifts at 4LG and 6LG might come from the effect of SEI/graphene and graphene/substrate interface. The chemical environment induced by these two interfaces might shift the energetics of the deintercalation process. As shown schematically in Figure S2, the impact of these interfaces decreases as FLG transitions into MLG by forming a better-defined bulk. We also note that differences in the background currents in Figure 3c,g−i, likely result from different contributions of each sample to their capacitive current and from residual SEI growth. SLG showed the lowest background current, reflecting its lowest activity toward reaction with Li and its lowest density of states which contribute to its capacitance. 4LG, 6LG, and MLG displayed a similar background current of 0.8, 0.3, and *ca.* 1.0 μA, respectively, which was observed to decrease with an increasing cycling number.

We note that the observed peaks in 6LG are broader than those in 4LG. We believe this is a consequence of the broader range of configurations and interactions available with a growing number of layers. Observing a progressive change is important in the context of the effects that turbostratic disorder, *i.e.*, random rotations and translations on pairs of graphene layers, potentially brings to the response of the lithium intercalation signal.[20] In the layer-by-layer transfer procedure used here, it is difficult to control turbostratic disorder; however, we believe that the existence of such disorder does not preclude the validity of the number of layer dependent observations done here. In the first place, 4LG and 6LG samples displayed marked voltammetric differences as a function of the number of layers, despite being produced using a common building material, *i.e.*, bilayer graphene. Even if the galleries formed by the layer-by-layer transfer stacking of two BLG sheets were less active than the ones formed by the native BLG, ionic interactions between Li^+ ions would still be expected to occur and to affect the electrostatic interactions perpendicular to the surface. Second, lithiation is capable of inducing the restacking of layers, provided the material is capable of accommodating the necessary structural changes.[20,37] As observed during our transfer procedure, "peeling off" of monolayer graphene is possible; thus, our layers are probably less bound than on natural graphite. This might facilitate structural changes after a few lithiation cycles and relieve some of the original turbostratic disorder. Finally, turbostratic disorder has been shown to strongly impact the amount of Li^+ that can be intercalated on carbons. The

DOI: 10.1021/acsnano.5b07692
ACS Nano 2016, 10, 4248−4257

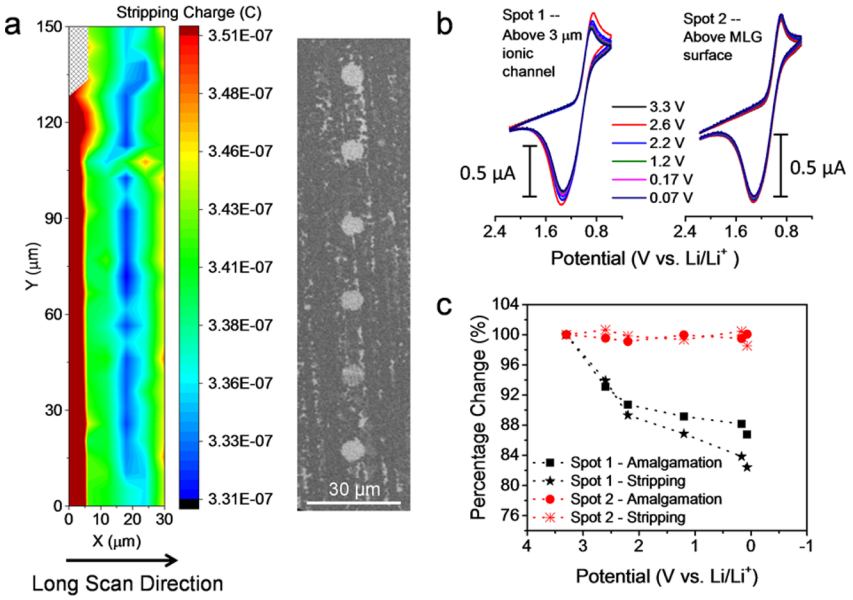

Figure 5. Li-ion flux study of MLG sample after SEI formation. (a) CV-SECM image of patterned MLG sample after SEI formation (left). Substrate was biased at 0.07 V to intercalate Li^+ for all experiments shown here. A series of CVs were taken at each position at 25 V/s with 5 μm steps, and each pixel is the integrated stripping charge of CV, which reflects amplified changes in the local Li^+ concentration. Blue-shifted signals represent areas of lower Li^+ concentration, therefore indicating a larger flux toward the substrate electrode. Their distribution matches with the patterned hole openings designed for Li^+ insertion. SEM image of a similar area is placed to the right for comparison. The X direction served as the long axis of the raster scan. The off-scale data (dark red color) and pixels where no data was taken (mesh pattern) in the first column of the image is likely an experimental or instrumental artifact. (b) Local stripping tip voltammograms showing the tip current as a function of tip potential over an active hole (left, on top of 3 μm ionic channel) and over the less active MLG surface (right), while the substrate activates Li^+ intercalation at various potentials imposed to the substrate. (c) Percentage change of amalgamation and stripping peak currents derived from panel b, showing the clear potential dependence of Li^+ flux into the holes but not on the MLG surface.

integrated charge of the deintercalation peaks in Figure 3h,i, shown in detail in Figure S3 and Table S1, yields the equivalents of Li^+ diffused into FLG planes. 4LG yielded a deintercalation charge of 12.2 μC (85% of calculated theoretical charge), and 6LG has 15.7 μC (65% of calculated theoretical charge). Both figures show evidence for a largely lithiated interface. Even with a relatively fast scan rate and turbostratic disordered structures, FLG can still maintain enough ability for Li insertion.[19,20,38] The observations provided in this article set a precedent in which new mechanistic insights derived from the transition of bulk graphite to an atomically thin interface can be explored.

In addition to its intercalation behavior, it is instructive to explore the similarities and differences in the electronic and ionic surface reactivity of graphene in the context of our current understanding of carbon materials. Specifically, we addressed the evolution of SEI conductivity and the role of the fabricated ionic-channels in facilitating Li ion intercalation. For this purpose, we used scanning electrochemical microscopy, a versatile tool for detecting reactivity at operating electrodes. To further explore the properties of the SEI, SECM operated in the feedback mode (Figure 4a) was used to image the spatially resolved rate of electron transfer of a patterned MLG electrode at various stages of SEI formation. According to the CVs of FLG (Figure 3), all electrodes displayed qualitatively the same SEI evolution process. Because MLG gave larger intercalation signatures, this electrode was chosen as representative of FLG samples to study SEI properties. When a nanodimensioned SECM tip was first approached to a pristine substrate of patterned multilayer graphene, positive feedback was observed, indicating that the substrate was electronically conductive, even at open circuit when unbiased (Figure 4c, black curve). SECM imaging was performed at various substrate potentials to observe the feedback response as a function of electrode activation.

Open circuit SECM images (E_{sub} ~ 3.3 V *vs* Li/Li^+) revealed nanoresolved features on the surface with clearly identifiable circular patterns on the substrate that correspond perfectly to the fabricated graphene patterns observed under SEM with the same center to center distances for the holes. SECM images were collected at progressively more negative substrate potentials at a tip−substrate distance of 133 nm. As pointed out through the dashed lines in Figure 4b, we chose conditions before, during, and after SEI formation, at 2.6, 1.2, and 0.07 V *vs* Li/Li^+, respectively. The SECM image at E_{sub} of 2.6 V (Figure 4d) shows good contrast between patterned holes and the MLG surface, with some contrast at defective regions that respond more to substrate overpotential. These defect regions have faster electron transfer kinetics than pristine graphene and have been observed previously *via* SECM[39] and with droplet based SECM probes.[40]

In following images, the substrate potential was ramped more negatively, now forming an SEI, which progressively showed a decreasing tip feedback response due to decreased substrate kinetics (Figure 4e,f). An overall decrease in tip current observed starting at E_{sub} of 1.2 V (Figure 4e) suggests the formation of a homogeneous SEI layer that partially hinders electron transfer at MLG surface. At E_{sub} of 0.07 V (Figure 4f), the pattern was indistinguishable, yielding only negative feedback to the tip signal. Negative feedback suggests a slowed-down regeneration of the mediator, indicative of lowered substrate kinetics that are unable to keep up with the mass transport imposed by the tip. We note that the impact of the SEI on electron transfer is opposite to that expected by a

DOI: 10.1021/acsnano.5b07692
ACS Nano 2016, 10, 4248−4257

large overpotential for the mediator regeneration reaction at the substrate. However, the growing SEI on the surface caused the surface to no longer be electronically conductive.[41−43] The contrasting behavior of the surface before and after SEI formation is also represented *via* feedback approach curves (Figure 4c). Imaging shows in larger detail that the original surface heterogeneity is eliminated after complete coverage of the substrate with the SEI (Figure 4f). The substrate was verified to still be electrochemically active after SECM imaging by measuring a voltammogram in which the intercalation of Li^+ is still clearly visible (Figure 4b, red curve). However, the SEI remained as a passivating layer, blocking electron transfer to TMPD even an image performed in the conditions of Figure 4d was repeated (Figure S4).

The intercalation of Li^+ on the graphene electrode was further verified using CV-SECM, an ionically sensitive technique capable of detecting the localized flux of Li^+ on an activated substrate. Our group recently introduced Hg-capped SECM tips for use in nonaqueous media for the imaging of lithium ions *via* redox competition.[28] In these previous experiments, the Hg-capped SECM tip senses the concentration of Li^+ in the electrolyte *via* an amalgamation process, *i.e.*, the formation of a Li(Hg) phase when the tip is poised at a sufficiently negative potential to reduce Li^+. If the tip is approached to, and rastered across a surface that actively intakes Li^+, the probe signal decreases as a result of the local decrease in Li^+ concentration. In addition to amalgamation, it is possible to operate the tip in stripping mode, where the accumulated Li in the amalgam is reversibly oxidized. The stripping charge displays a linear relationship with concentration.[28] Operating the tip in stripping mode is advantageous because the small Hg cap does not get saturated with Li, and because the local Li^+ concentration is continuously replenished by the sweeping action of the probe. We build upon these previous studies and incorporate a powerful methodology where continuously scanned SECM images are broken up into individual pixels and every pixel is a stationary fast scan cyclic voltammogram measuring stripping voltammetry.[44−47] The SECM tip was moved step by step at 5 μm intervals, and CVs were collected at each pixel at 25 V/s. The integrated stripping charge was plotted in every pixel. This type of stop-and-go based CV-SECM imaging is rich in experimental data and yields more data per line scan than traditional SECM imaging.

Each pixel in the CV-SECM image (Figure 5a, left) collected with our mercury probes corresponds to the stripping charge calculated from the integrated current of stripping Li^+. While the mercury capped SECM tip was measuring stripping voltammetry at every pixel, the substrate was continuously poised at 0.07 V in order to have intercalation of Li^+ occur. While a constant background is present in the entire image due to a flux of Li^+ from the electrolyte into the probe, the spots in the CV-SECM image that have the lowest stripping charge correspond to regions on the substrate that give the most competition for the local source of Li^+ and are seen in blue. This scheme of redox competition has previously been used in SECM to generate high resolution images that do not require the tip to be extremely close to the substrate.[48,49] The blue spots in the CV-SECM image match well with the spatial distribution of the etched openings in the graphene pattern (Figure 5a, left), showing that the substrate design is indeed facilitating Li^+ intercalation and that the formation of the SEI is not consuming the underlying active material. To further demonstrate this effect at specific sites, the Hg probe was placed directly on top of both a hole opening area and flat MLG surface. SECM tip CVs at various substrate potential were collected at each described spot and are listed in Figure 5b with their amalgamation and stripping peak current changes shown in Figure 5c. A decrease for both amalgamation and stripping currents was observed at the etched holes, which contain edge plane openings that induce strong competition for Li^+ at these sites. In contrast, stripping CVs right above MLG basal planes remained constant without any dependence on substrate potential. Collectively, these observations demonstrate that Li ions migrate into graphene interlayers more efficiently through the edge planes. This work would be the first time that SECM has been used to visualize ionic fluxes through an SEI on a battery material in real time, and help validate results suggesting that FLG electrodes are a viable platform for studying fundamental intercalation effects on graphitic materials.

CONCLUSIONS

In this work, we used few-layer graphene, both directly growth and layer-by-layer transferred, to explore Li^+ intercalation on an atomically thin interface. Li^+ insertion in FLG follows a staging mechanism, reminiscent of graphite, but the limited number of graphene sheets cause significant deviations in the intercalation mechanism, as evaluated *via* cyclic voltammetry. Due to the physical restriction, no Li intercalation was found in single-layer graphene sample. In FLG less than 5 layers, 4LG as example, only stage 1−3 can be resolved. In spite of potential difference of intercalation/deintercalation, 6LG already exhibit similar staging mechanism as ∼10 layer MLG and graphite. This work verifies the universality of staging mechanism in layered carbonaceous materials, and it provides insight into the early state Li^+ intercalation process in graphene-type materials. Additionally, this work also opens interesting avenues in the control of ion insertion mechanisms and insertion energies *via* electrode nanostructuring.

As a spatially resolved electrochemical probing platform, SECM provided information on both the electronic and ionic reactivity of the graphene substrate. SECM feedback images monitored the impact of SEI formation under different substrate bias, until the stable and condensed SEI layer totally blocked electron transfer. In contrast, CV-SECM experiments using a Hg-capped Pt tip as Li^+ sensitive ionic probe were applied to demonstrate that electrode patterning leads to points of access for Li^+ intercalation preferentially on regions where the edge plane of graphene is exposed. Current efforts in our laboratory will focus on increasing the temporal and spatial resolution of CV-SECM methods for exploring ionic pathways within defects on the SEI. This work highlights the impact of nanostructure and microstructure on macroscopic electrochemical behavior and opens the door to the mechanistic control of ion intercalation using graphene, an atomically thin interface where surface and bulk reactivity converge.

EXPERIMENTAL PROCEDURES

Chemicals. All chemicals were purchased from commercial sources and used as received. Propylene carbonate (PC, anhydrous, 99.7%), ethylene carbonate (EC, anhydrous, 99%), lithium tetrafluoroborate ($LiBF_4$, 98%), silver nitrate ($AgNO_3$, 99%), mercury(II) chloride ($HgCl_2$, 99.5%), *N*,*N*,*N*′,*N*′-tetramethyl-*p*-phenylenediamine (TMPD, 99%), acetone (99.5%), isopropyl alcohol (IPA 99.5%), glacial acetic acid (99.5%), and ethylenediaminetetraacetic acid disodium salt dihydrate ($Na_2EDTA{\cdot}2H_2O$, 99.0%) were all purchased from Sigma-

DOI: 10.1021/acsnano.5b07692
ACS Nano 2016, 10, 4248−4257

Aldrich. Twenty-five micrometers thick copper foil was purchased from Alfa Aesar. Nano 950 K A4 PMMA, 495 K A2 PMMA, and Microposit S1813 photoresist were purchased from MicroChem. AZ 917 MIF developer was purchased from AZ Electronic Materials. CE-100 Copper etchant was purchased from Transene Company. SiO_2/Si wafer (3 in. B-doped P-type Si wafer with 300 nm wet thermal oxide) was purchased from University Wafer. The deionized water (DI water) was filtered using a Millipore system.

Graphene Growth Procedure. Multilayer graphene and bilayer graphene were grown by chemical vapor deposition (CVD) using methane and 25 μm Cu foil as catalyst. Prior to growth, the Cu foil was treated in acetone (10 s), water (10 s), glacial acetic acid (10 min), water (10 s), acetone (10 s), and IPA (10 s) to remove any surface oxides. The Cu foil was then mounted in CVD chamber for graphene growth with different recipes. Bilayer graphene was grown with previously established recipe[50] at 0.04 Torr with two steps: annealing under 1000 °C, 1000 sccm Ar and 50 sccm H_2 for 30 min; graphene growing at 1000 °C, 100 sccm CH_4 and 50 sccm H_2 for 25 min. Multilayer graphene was grown using a modified recipe from previously reported atmosphere pressure CVD method[51] with no annealing step and growth at 960 °C, 10 sccm CH_4 and 30 sccm H_2 for 5 min.

Graphene Transfer. CVD grown graphene was transferred onto different substrates (SiO_2/Si wafer, and glass) through a wet transfer method. After graphene growth, one side of the Cu foil with graphene was protected with 1 layer of 495 K A2 PMMA and 2 layers of 950 K A4 PMMA *via* spin-coating at 3000 rpm for 30 s. The protected graphene was floated on top of Cu etchant for 4 h at 40 °C to remove Cu foil beneath the graphene. The floating graphene/PMMA sheet went through 4 rinse steps with DI water, 1 h treatment with 0.1 M Na_2EDTA aqueous solution, and 4 rinse steps with DI water again to fully remove any metal residue. The clean graphene/PMMA sheet was finally transferred onto the desired substrate and blow dried under Argon. Additional organic solvent treatments were then applied to remove PMMA protecting layer: 2 h in anisole, 4 h in dichloromethane/acetone mixture (1:1 ratio), and 2 h in isopropyl alcohol. Repetition of this process yields multilayered graphene samples.

Patterning Graphene. Photolithography and reactive ion etching (RIE) methods were applied to define and create two-dimensional micron patterns on graphene. For photolithography, positive photoresist S1813 was selected to create patterned openings, 3 μm square array with 24 μm center-to-center distance, on graphene. S1813 layer was spin coated onto graphene at 4000 rpm for 45 s and soft baked at 115 °C for 1.5 min. Karl Suss MJB3 contact mask aligner was used to transfer the pattern from the mask to the photoresist layer. After developing in AZ 917 MIF developer for 15 s, 3 μm square array openings were created on top of graphene. A Plasma Lab Freon/O_2 RIE system was applied to selectively etch the exposed graphene area under 20 sccm O_2, 37 mW RF energy and 40 mTorr pressure for 30 s. The etched graphene sample was carefully rinsed with acetone to remove photoresist layer which left a pristine patterned graphene on the substrate.

Sample Characterization. Graphene samples were characterized *via* optical microscopy (Zeiss Axio Lab.A1, Germany), scanning electron microscopy (SEM, Hitachi S-4800 high resolution SEM, Japan), Raman spectroscopy (Nanophoton Laser Raman Microscope RAMAN-11, Japan), and UV−vis spectroscopy (Shimadzu, Japan). Raman measurements were used in both spectroscopic and imaging modes.

Electrochemical Test. All electrochemical experiments were conducted using a CHI 920D SECM from CH Instruments (Austin, TX) inside of a glovebox (MBraun, Stratham, NH) with mindful control of the oxygen and water levels in the atmosphere to be less than 0.1 ppm, respectively. A Pt wire and an Ag/Ag^+ (0.1 M $AgNO_3$ in a 50:50 mixture of PC/EC) electrode were used as the counter and reference electrodes. A 0.1 M $LiBF_4$ solution in 50:50 PC/EC mixture was used as stock solution.

Li Intercalation with Cyclic Voltammetry (CV). We chose slow scan CV to obtain Li intercalation information into graphene samples. Different graphene samples (MLG, patterned SLG, 4LG, 6LG) were used as working electrode, with a SECM Teflon cell defined working area of 4.9 mm^2. After adding stock solution, CVs were taken at low scan rate of 1 mV/s over multiple cycles to test SEI formation and Li intercalation processes.

Nano-SECM Feedback Imaging. Nanometer sized SECM tips with a 300 nm radius platinum electrode were fabricated using Wollaston wire with an RG of approximately 25; the detailed fabrication procedure is listed in Supporting Information. Fresh MLG with patterned 3 μm openings was used to explore SEI electronic conductivity characteristics. The Wollaston wire electrodes were approached to the patterned graphene substrate in the feedback mode of SECM using a solution of 10 mM TMPD in stock solution as an electrochemical mediator. SECM images were collected at various substrate bias steps from open circuit (3.3 V) to SEI fully formed (0.07 V) to monitor surface kinetics changes as the SEI is formed on fresh MLG samples.

CV-SECM Imaging. The 5 μm radius platinum electrodes (RG ~ 2) were purchased from CH Instruments (Austin, TX). Mercury capped SECM tips were fabricated inside of the glovebox from a nonaqeuous solution by depositing mercury on the surface from a 0.1 M solution of $HgCl_2$ with 0.1 M $TBAPF_6$ in DMF through a chronoamperometric step at −0.8 V *vs* a tungsten wire for 144 s to deposit 34 μC (0.34 nmol) of mercury on the surface. The presence of mercury on the SECM tip was verified by performing stripping voltammetry in the presence of the electrolyte used for lithium intercalation for the patterned graphene (0.1 M $LiBF_4$). Stripping voltammetry showed clean and clear amalgamation formation for lithium at 1 V *vs* Li/Li^+ with reversible stripping.

The tip was approached to the surface with 10 mM TMPD using only the first oxidation as mercury itself will strip off the surface if the second oxidation is accessed. Cyclic voltammetry SECM (CV-SECM) imaging was performed by measuring 3 complete cyclic voltammograms at 25 V/s to show the amalgamation and stripping of Li^+ at every single pixel in the image where every pixel was 5 μm large. The last voltammogram measured at every pixel was integrated to find the stripping charge and plotted as a function of surface location to generate a CV-SECM image.

ASSOCIATED CONTENT

Supporting Information

The Supporting Information is available free of charge on the ACS Publications website at DOI: 10.1021/acsnano.5b07692.

Details of Wollaston tip fabrication procedure, CVs of unpatterned BLG, 4LG and HOPG, SECM open circuit image of fresh MLG sample, calculation of intercalated charge of 4LG and 6LG, and open circuit SECM feedback image after SEI formation (PDF)

AUTHOR INFORMATION

Corresponding Author

*E-mail: joaquinr@illinois.edu.

Notes

The authors declare no competing financial interest.

ACKNOWLEDGMENTS

The authors acknowledge the University of Illinois for generous start-up funds. M.B. acknowledges support by the National Science Foundation Graduate Research Fellowship Program under Grant No. DGE-1144245. Any opinions, findings, and conclusions or recommendations expressed in this material are those of the authors and do not necessarily reflect the views of the National Science Foundation. Sample preparation and characterization were carried out in part in the Frederick Seitz Materials Research Laboratory Central Facilities and the Micro and Nanotechnology Laboratory, University of Illinois. The

DOI: 10.1021/acsnano.5b07692
ACS Nano 2016, 10, 4248−4257

authors would like to thank our group member Zachary J. Barton, for help in developing the implementation of the employed CV-SECM technique.

REFERENCES

(1) Yazami, R.; Touzain, P. A Reversible Graphite Lithium Negative Electrode for Electrochemical Generators. *J. Power Sources* **1983**, *9*, 365−371.
(2) Levi, M. D.; Aurbach, D. The Mechanism of Lithium Intercalation in Graphite Film Electrodes in Aprotic Media. Part 1. High Resolution Slow Scan Rate Cyclic Voltammetric Studies and Modeling. *J. Electroanal. Chem.* **1997**, *421*, 79−88.
(3) Levi, M. D.; Levi, E. A.; Aurbach, D. The Mechanism of Lithium Intercalation in Graphite Film Electrodes in Aprotic Media. Part 2. Potentiostatic Intermittent Titration and *in situ* XRD Studies of the Solid-State Ionic Diffusion. *J. Electroanal. Chem.* **1997**, *421*, 89−97.
(4) Verma, P.; Maire, P.; Novák, P. A Review of the Features and Analyses of the Solid Electrolyte Interphase in Li-Ion Batteries. *Electrochim. Acta* **2010**, *55*, 6332−6341.
(5) Agubra, V. A.; Fergus, J. W. The Formation and Stability of the Solid Electrolyte Interface on the Graphite Anode. *J. Power Sources* **2014**, *268*, 153−162.
(6) Zhang, S.; Ding, M. S.; Xu, K.; Allen, J.; Jow, T. R. Understanding Solid Electrolyte Interface Film Formation on Graphite Electrodes. *Electrochem. Solid-State Lett.* **2001**, *4*, A206−A208.
(7) Herstedt, M.; Stjerndahl, M.; Gustafsson, T.; Edström, K. Anion Receptor for Enhanced Thermal Stability of the Graphite Anode Interface in a Li-Ion Battery. *Electrochem. Commun.* **2003**, *5*, 467−472.
(8) Aurbach, D.; Markovsky, B.; Weissman, I.; Levi, E.; Ein-Eli, Y. On the Correlation Between Surface Chemistry and Performance of Graphite Negative Electrodes for Li Ion Batteries. *Electrochim. Acta* **1999**, *45*, 67−86.
(9) Etacheri, V.; Marom, R.; Elazari, R.; Salitra, G.; Aurbach, D. Challenges in the Development of Advanced Li-Ion Batteries: a Review. *Energy Environ. Sci.* **2011**, *4*, 3243−3262.
(10) Petnikota, S.; Rotte, N.; Srikanth, V. S. S.; Kota, B. R.; Reddy, M. V.; Loh, K.; Chowdari, B. V. R. Electrochemical Studies of Few-Layered Graphene as an Anode Material for Li Ion Batteries. *J. Solid State Electrochem.* **2014**, *18*, 941−949.
(11) Pollak, E.; Geng, B.; Jeon, K.-J.; Lucas, I. T.; Richardson, T. J.; Wang, F.; Kostecki, R. The Interaction of Li^+ with Single-Layer and Few-Layer Graphene. *Nano Lett.* **2010**, *10*, 3386−3388.
(12) Lee, E.; Persson, K. A. Li Absorption and Intercalation in Single Layer Graphene and Few Layer Graphene by First Principles. *Nano Lett.* **2012**, *12*, 4624−4628.
(13) Liang, Y. T.; Hersam, M. C. Towards Rationally Designed Graphene-Based Materials and Devices. *Macromol. Chem. Phys.* **2012**, *213*, 1091−1100.
(14) Geim, A. K. Graphene: Status and Prospects. *Science* **2009**, *324*, 1530−1534.
(15) Geim, A. K.; Novoselov, K. S. The Rise of Graphene. *Nat. Mater.* **2007**, *6*, 183−191.
(16) Liao, L.; Peng, H.; Liu, Z. Chemistry Makes Graphene beyond Graphene. *J. Am. Chem. Soc.* **2014**, *136*, 12194−12200.
(17) Dahn, J. R. Phase Diagram of Li_xC_6. *Phys. Rev. B: Condens. Matter Mater. Phys.* **1991**, *44*, 9170−9177.
(18) Song, M. K.; Hong, S. D.; No, K. T. The Structure of Lithium Intercalated Graphite Using an Effective Atomic Charge of Lithium. *J. Electrochem. Soc.* **2001**, *148*, A1159−A1163.
(19) Zheng, T.; Dahn, J. R. Effect of Turbostratic Disorder on the Staging Phase Diagram of Lithium-Intercalated Graphitic Carbon Hosts. *Phys. Rev. B: Condens. Matter Mater. Phys.* **1996**, *53*, 3061−3071.
(20) Zheng, T.; Reimers, J. N.; Dahn, J. R. Effect of Turbostratic Disorder in Graphitic Carbon Hosts on the Intercalation of Lithium. *Phys. Rev. B: Condens. Matter Mater. Phys.* **1995**, *51*, 734−741.
(21) Levi, M. D.; Aurbach, D. Simultaneous Measurements and Modeling of the Electrochemical Impedance and the Cyclic Voltammetric Characteristics of Graphite Electrodes Doped with Lithium. *J. Phys. Chem. B* **1997**, *101*, 4630−4640.
(22) Ritzert, N. L.; Rodriguez-Lopez, J.; Tan, C.; Abruna, H. D. Kinetics of Interfacial Electron Transfer at Single-Layer Graphene Electrodes in Aqueous and Nonaqueous Solutions. *Langmuir* **2013**, *29*, 1683−1694.
(23) Eshkenazi, V.; Peled, E.; Burstein, L.; Golodnitsky, D. XPS Analysis of the SEI Formed on Carbonaceous Materials. *Solid State Ionics* **2004**, *170*, 83−91.
(24) Lee, J. T.; Nitta, N.; Benson, J.; Magasinski, A.; Fuller, T. F.; Yushin, G. Comparative Study of the Solid Electrolyte Interphase on Graphite in Full Li-Ion Battery Cells Using X-Ray Photoelectron Spectroscopy, Secondary Ion Mass Spectrometry, and Electron Microscopy. *Carbon* **2013**, *52*, 388−397.
(25) Santner, H. J.; Korepp, C.; Winter, M.; Besenhard, J. O.; Möller, K. C. In-situ FTIR Investigations on the Reduction of Vinylene Electrolyte Additives Suitable for Use in Lithium-Ion Batteries. *Anal. Bioanal. Chem.* **2004**, *379*, 266−271.
(26) Chattopadhyay, S.; Lipson, A. L.; Karmel, H. J.; Emery, J. D.; Fister, T. T.; Fenter, P. A.; Hersam, M. C.; Bedzyk, M. J. *In Situ* X-ray Study of the Solid Electrolyte Interphase (SEI) Formation on Graphene as a Model Li-ion Battery Anode. *Chem. Mater.* **2012**, *24*, 3038−3043.
(27) Zhang, S. S.; Xu, K.; Jow, T. R. EIS Study on the Formation of Solid Electrolyte Interface in Li-Ion Battery. *Electrochim. Acta* **2006**, *51*, 1636−1640.
(28) Barton, Z. J.; Rodriguez-Lopez, J. Lithium Ion Quantification Using Mercury Amalgams as *in Situ* Electrochemical Probes in Nonaqueous Media. *Anal. Chem.* **2014**, *86*, 10660−10667.
(29) Graf, D.; Molitor, F.; Ensslin, K.; Stampfer, C.; Jungen, A.; Hierold, C.; Wirtz, L. Spatially Resolved Raman Spectroscopy of Single- and Few-Layer Graphene. *Nano Lett.* **2007**, *7*, 238−242.
(30) Li, X. S.; Cai, W. W.; An, J. H.; Kim, S.; Nah, J.; Yang, D. X.; Piner, R.; Velamakanni, A.; Jung, I.; Tutuc, E.; Banerjee, S. K.; Colombo, L.; Ruoff, R. S. Large-Area Synthesis of High-Quality and Uniform Graphene Films on Copper Foils. *Science* **2009**, *324*, 1312−1314.
(31) Bae, S.; Kim, H.; Lee, Y.; Xu, X.; Park, J.-S.; Zheng, Y.; Balakrishnan, J.; Lei, T.; Ri Kim, H.; Song, Y. I.; Kim, Y.-J.; Kim, K. S.; Ozyilmaz, B.; Ahn, J.-H.; Hong, B. H.; Iijima, S. Roll-to-Roll Production of 30-in. Graphene Films for Transparent Electrodes. *Nat. Nanotechnol.* **2010**, *5*, 574−578.
(32) Nair, R. R.; Blake, P.; Grigorenko, A. N.; Novoselov, K. S.; Booth, T. J.; Stauber, T.; Peres, N. M. R.; Geim, A. K. Fine Structure Constant Defines Visual Transparency of Graphene. *Science* **2008**, *320*, 1308.
(33) Ishigami, M.; Chen, J. H.; Cullen, W. G.; Fuhrer, M. S.; Williams, E. D. Atomic Structure of Graphene on SiO_2. *Nano Lett.* **2007**, *7*, 1643−1648.
(34) Nie, M.; Chalasani, D.; Abraham, D. P.; Chen, Y.; Bose, A.; Lucht, B. L. Lithium Ion Battery Graphite Solid Electrolyte Interphase Revealed by Microscopy and Spectroscopy. *J. Phys. Chem. C* **2013**, *117*, 1257−1267.
(35) Sole, C.; Drewett, N. E.; Liu, F.; Abdelkader, A. M.; Kinloch, I. A.; Hardwick, L. J. The Role of Re-Aggregation on the Performance of Electrochemically Exfoliated Many-Layer Graphene for Li-Ion Batteries. *J. Electroanal. Chem.* **2015**, *753*, 35−41.
(36) Yamada, Y.; Miyazaki, K.; Abe, T. Role of Edge Orientation in Kinetics of Electrochemical Intercalation of Lithium-Ion at Graphite. *Langmuir* **2010**, *26*, 14990−14994.
(37) Boehm, R. C.; Banerjee, A. Theoretical Study of Lithium Intercalated Graphite. *J. Chem. Phys.* **1992**, *96*, 1150−1157.
(38) Dahn, J. R.; Sleigh, A. K.; Shi, H.; Reimers, J. N.; Zhong, Q.; Way, B. M. Dependence of the Electrochemical Intercalation of Lithium in Carbons on the Crystal-Structure of the Carbon. *Electrochim. Acta* **1993**, *38*, 1179−1191.
(39) Tan, C.; Rodríguez-López, J.; Parks, J. J.; Ritzert, N. L.; Ralph, D. C.; Abruña, H. D. Reactivity of Monolayer Chemical Vapor

DOI: 10.1021/acsnano.5b07692
ACS Nano 2016, 10, 4248−4257

Deposited Graphene Imperfections Studied Using Scanning Electrochemical Microscopy. *ACS Nano* **2012**, *6*, 3070−3079.
(40) Guell, A. G.; Cuharuc, A. S.; Kim, Y. R.; Zhang, G. H.; Tan, S. Y.; Ebejer, N.; Unwin, P. R. Redox-Dependent Spatially Resolved Electrochemistry at Graphene and Graphite Step Edges. *ACS Nano* **2015**, *9*, 3558−3571.
(41) Zampardi, G.; La Mantia, F.; Schuhmann, W. Determination of the Formation and Range of Stability of the SEI on Glassy Carbon by Local Electrochemistry. *RSC Adv.* **2015**, *5*, 31166−31171.
(42) Zampardi, G.; La Mantia, F.; Schuhmann, W. In-Operando Evaluation of the Effect of Vinylene Carbonate on the Insulating Character of the Solid Electrolyte Interphase. *Electrochem. Commun.* **2015**, *58*, 1−5.
(43) Zampardi, G.; Ventosa, E.; La Mantia, F.; Schuhmann, W. *In Situ* Visualization of Li-Ion Intercalation and Formation of the Solid Electrolyte Interphase on TiO_2 Based Paste Electrodes Using Scanning Electrochemical Microscopy. *Chem. Commun.* **2013**, *49*, 9347−9349.
(44) Alpuche-Aviles, M. A.; Baur, J. E.; Wipf, D. O. Imaging of Metal Ion Dissolution and Electrodeposition by Anodic Stripping Voltammetry-Scanning Electrochemical Microscopy. *Anal. Chem.* **2008**, *80*, 3612−3621.
(45) Diaz-Ballote, L.; Alpuche-Aviles, M.; Wipf, D. O. Fast-Scan Cyclic Voltammetry-Scanning Electrochemical Microscopy. *J. Electroanal. Chem.* **2007**, *604*, 17−25.
(46) Chen, C. H.; Jacobse, L.; McKelvey, K.; Lai, S. C. S.; Koper, M. T. M.; Unwin, P. R. Voltammetric Scanning Electrochemical Cell Microscopy: Dynamic Imaging of Hydrazine Electro-oxidation on Platinum Electrodes. *Anal. Chem.* **2015**, *87*, 5782−5789.
(47) Takahashi, Y.; Kumatani, A.; Munakata, H.; Inomata, H.; Ito, K.; Ino, K.; Shiku, H.; Unwin, P. R.; Korchev, Y. E.; Kanamura, K.; Matsue, T. Nanoscale Visualization of Redox Activity at Lithium-Ion Battery Cathodes. *Nat. Commun.* **2014**, *5*, 5450.
(48) Eckhard, K.; Chen, X. X.; Turcu, F.; Schuhmann, W. Redox Competition Mode of Scanning Electrochemical Microscopy (RC-SECM) for Visualisation of Local Catalytic Activity. *Phys. Chem. Chem. Phys.* **2006**, *8*, 5359−5365.
(49) Zoski, C. G.; Aguilar, J. C.; Bard, A. J. Scanning Electrochemical Microscopy. 46. Shielding Effects on Reversible and Quasireversible Reactions. *Anal. Chem.* **2003**, *75*, 2959−2966.
(50) Cristarella, T. C.; Chinderle, A. J.; Hui, J.; Rodríguez-López, J. Single-Layer Graphene as a Stable and Transparent Electrode for Nonaqueous Radical Annihilation Electrogenerated Chemiluminescence. *Langmuir* **2015**, *31*, 3999−4007.
(51) Tu, Z.; Liu, Z.; Li, Y.; Yang, F.; Zhang, L.; Zhao, Z.; Xu, C.; Wu, S.; Liu, H.; Yang, H.; Richard, P. Controllable Growth of 1−7 Layers of Graphene by Chemical Vapour Deposition. *Carbon* **2014**, *73*, 252−258.

DOI: 10.1021/acsnano.5b07692
ACS Nano 2016, 10, 4248−4257